

Treadmilling of actin filaments via Brownian dynamics simulations

Kunkun Guo,^{1,2,a)} Julian Shillcock,^{1,3} and Reinhard Lipowsky^{1,b)}

¹Theory and Biosystems, Max Planck Institute of Colloids and Interfaces, 14424 Potsdam, Germany

²College of Materials Science and Engineering, Hunan University, Changsha, 410082, People's Republic of China

³MEMPHYS-Centre for Biomembrane Physics, University of Southern Denmark, Campusvej 55, 5230 Odense M, Denmark

(Received 3 June 2010; accepted 15 September 2010; published online 19 October 2010)

Actin polymerization is coupled to the hydrolysis of adenosine triphosphate (ATP) into adenosine diphosphate (ADP) and inorganic phosphate (P_i). Therefore, each protomer within an actin filament can attain three different nucleotide states corresponding to bound ATP, ADP/ P_i , and ADP. These protomer states form spatial patterns on the growing (or shrinking) filaments. Using Brownian dynamics simulations, the growth behavior of long filaments is studied, together with the associated protomer patterns, as a function of ATP-actin monomer concentration, C_T , within the surrounding solution. For concentrations close to the critical concentration $C_T = C_{T,cr}$, the filaments undergo treadmilling, i.e., they grow at the barbed and shrink at the pointed end, which leads to directed translational motion of the whole filament. The corresponding nonequilibrium states are characterized by several global fluxes and by spatial density and flux profiles along the filaments. We focus on a certain set of transition rates as deduced from *in vitro* experiments and find that the associated treadmilling (or turnover) rate is about 0.08 monomers per second. © 2010 American Institute of Physics. [doi:10.1063/1.3497001]

I. INTRODUCTION

The polymerization of actin monomers (or G-actin) into actin filaments is important for many biological processes such as cell division, motility, reproduction, and endocytosis.¹⁻⁴ The coupling of this polymerization process to adenosine triphosphate (ATP) hydrolysis implies that each protomer within an actin filament (or F-actin) can attain three different nucleotide states corresponding to bound ATP, ADP/ P_i , and adenosine diphosphate (ADP).

Actin filaments are polar and have two distinct ends, a barbed and a pointed end, reflecting the polarity of the actin monomers that attach to both filament ends but do so with different attachment rates. Furthermore, the terminal protomers at the filament ends exhibit different detachment rates corresponding to the three possible nucleotide states of these protomers.⁵⁻⁷ Therefore, when the filaments are suspended in a solution of ATP-actin monomers, their growth is governed by two attachment rates and six detachment rates.

Since the attachment rates depend on the concentration C_T of free ATP-actin monomers, the growth rates at the two filament ends vary with this concentration as well. For a certain range of concentrations, the filament grows at the barbed end and simultaneously shrinks at the pointed end. The latter process, known as treadmilling or filament turnover,^{3,8,9} can be viewed as an effective reshuffling of protomers from one filament end to the other end, which leads to a displacement of the whole filament in the direction of the barbed end. Such a directed displacement is only possible because the filament growth is coupled to ATP hydroly-

sis and because this latter reaction is not in chemical equilibrium with ATP synthesis. At the steady state critical concentration $C_T = C_{T,cr}$, the growth rate at the barbed end is equal to the shrinkage rate at the pointed end, and the treadmilling filament attains a constant average length.¹⁰

In vivo, actin polymerization is a rather complex process with the participation of many other proteins that bind to G- and/or F-actin. Here, we will focus on *in vitro* experiments that have revealed many fascinating aspects of actin treadmilling^{3,11} which has even been observed for individual filaments,¹² but the molecular mechanisms underlying this process remain to be elucidated.

Previous theoretical work on actin polymerization coupled to ATP hydrolysis was primarily based on rate equations¹³⁻¹⁶ and stochastic simulations.¹⁷⁻¹⁹ In this article, we use particle-based computer simulations to study actin polymerization and the associated treadmilling process. Relatively short filament segments can be investigated by molecular dynamics simulations, which have shown that electrostatic interactions play a role in guiding the monomers onto the ends of the filament.^{20,21} However, because of their high computational cost, these highly detailed simulations have been limited to actin tetramers. In order to study the growth and treadmilling of long actin filaments, we have developed a Brownian dynamics algorithm that is able to overcome the large separation of time scales between relatively fast monomer diffusion and relatively slow monomer attachment and detachment events.²² We have previously shown that our approach can be used to study the polymerization and depolymerization of ADP-actin. In the present article, we apply this approach in order to elucidate the coupling between ATP-actin polymerization and ATP hydrolysis.

^{a)}Electronic mail: kunkunguo@gmail.com.

^{b)}Electronic mail: lipowsky@mpikg.mpg.de

Several possible mechanisms for the coupling between actin polymerization and ATP hydrolysis have been proposed and studied theoretically: random,^{5,17,19,23} vectorial,^{16,19,24,25} and cooperative hydrolysis.^{19,24,26} Here, we consider the simplest mechanism corresponding to random hydrolysis, for which both the ATP cleavage rate and the phosphate release rate are taken to be independent of the local neighborhoods of the corresponding protomers.

Our article is organized as follows. First, we describe our theoretical approach for the different processes involved in actin polymerization coupled to ATP hydrolysis. Second, we simulate ensembles of filaments and determine the overall growth rate of the filament as a function of free ATP-actin monomer concentration C_T . We use two different methods to calculate the overall growth rate: (i) We measure the filament length as a function of time and determine the growth rate from the first derivative of the filament length with respect to time; and (ii) we determine the average waiting times for attachment and detachment at the two filament ends and express the overall growth rate in terms of these waiting times. From these waiting times, we estimate the treadmilling (or turnover) rate close to the critical concentration, at which the overall growth rate vanishes. We show that the critical concentration is strongly affected by the P_i release rate of ADP/ P_i -actin monomers. In addition, we determine a variety of other quantities that are difficult to measure experimentally but provide nontrivial crosschecks on the consistency of our simulations: the probabilities for the terminal protomers to be in the different nucleotide states; the density and flux profiles along the filament; and the average number of ATP-actin and ADP/ P_i -actin protomers at the two filament ends.

In principle, one should distinguish three different critical concentrations: the critical concentration $C_{T,cr}$ of the whole filament, also called steady state critical concentration, as well as the critical concentrations of the barbed and of the pointed filament ends. However, for the transition rates as reported in Ref. 23 and used here, all rates at the pointed end are much smaller than the corresponding rates at the barbed end, which implies that the values of the three critical concentrations are quite similar, and leads to a rather narrow treadmilling regime close to the critical concentration $C_{T,cr}$.

II. THEORETICAL APPROACH

A. Basic aspects of coarse-grained description

The different processes involved in actin polymerization coupled to ATP hydrolysis are illustrated in Fig. 1. The initial filament consists of 200 ADP-actin protomers and is placed in a simulation box that contains a certain concentration C_T of freely diffusing ATP-actin monomers. A coarse-grained model is used in which the monomers are constructed from three Brownian particles that are connected into an equilateral triangle.²² These monomers undergo unbiased diffusion as simulated by Brownian dynamics and can attach to the filament if they enter the conelike capture zones in front of the two filament ends, see Fig. 1.

As shown in Ref. 22, the attachment events induced by these capture zones are governed by exponential waiting time distributions and, thus, represent Markov processes,

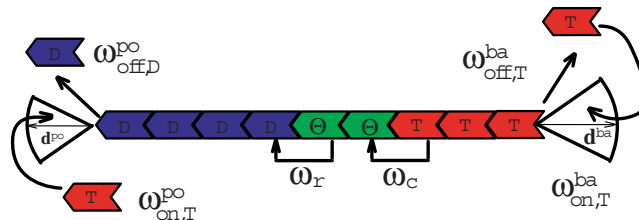


FIG. 1. Schematic view of the different processes that determine the time evolution of actin polymerization and ATP hydrolysis. Actin monomers and protomers with a bound ATP, ADP/ P_i , and ADP molecule are denoted by T , Θ and D , respectively. The two conical regions at the barbed (right) and pointed (left) end of the filament have linear dimensions d^{ba} and d^{po} . These regions represent capture zones for the diffusing T monomers and determine the attachment rates $\omega_{on,T}^{ba}$ and $\omega_{on,T}^{po}$ for these monomers at the two ends. The T protomers of the filament are transformed into Θ protomers with the ATP cleavage rate ω_c , the Θ protomers are changed into D protomers with the P_i release rate ω_r . The two terminal protomers at the two filament ends can also detach from the filament as illustrated for a T protomer at the barbed end and for a D protomer at the pointed end. Since both terminal protomers can attain three different nucleotide states, one has to distinguish six detachment rates, see text.

which could also be modeled by a Gillespie algorithm as used, e.g., in Ref. 19. The explicit description via capture zones has the advantage, however, that it allows us to consider more complex geometries such as filament bundles and/or confining walls, for which some of the filament ends may be partially shielded from the diffusing monomers.

When a monomer binds to the filament, a new ATP-actin monomer is added to the simulation box far from the filament so that the bulk concentration of the free monomers remains constant. After an ATP-monomer has been incorporated into the filament, it is turned into an ATP-actin protomer. Within the filament, the protomers are connected by harmonic bond potentials in such a way that they form a triangular column or stack. The triangular geometry acts to enhance the bending stiffness of the filament, which is incorporated by an additional three-body potential between three adjacent triangles. Thus, the helical (or “double-stranded”) structure of real F-actin is ignored in the coarse-grained model used here. A more detailed description of the molecular architecture and the different interactions between the Brownian particles has been previously given in Ref. 22.

Once an ATP-actin monomer has been turned into an ATP-actin protomer, it may be further transformed into an ADP/ P_i -actin protomer by ATP cleavage and subsequently into an ADP-actin protomer by P_i release. At the barbed and pointed ends, the hydrolysis of the terminal protomers competes with the detachment of these protomers. As in our previous study,²² the newly detached protomers are removed from the solution in order to avoid too frequent reattachments to the filament. This removal step is related to our rescaling procedure as explained further below.

In the following, we will use the abbreviations T , Θ , and D for the three species ATP-actin, ADP/ P_i -actin, and ADP-actin, as well as the superscripts “ba” and “po” for the barbed and pointed ends, respectively. In order to combine two equations that have the same form both at the barbed and at the pointed end, we will also use the superscript (α) which has the two values (α)=ba and (α)=po.

TABLE I. Numerical values for the different transition rates as used in the simulations: Attachment rate constants κ_{on} for T monomers; detachment rates ω_{off} for T , Θ , and D protomers; ATP cleavage rate ω_c ; and P_i release rate ω_r . All rates are given in units of 1/s, all rate constants κ in units of $1/(\mu\text{M s})$. The superscripts ba and po refer to the barbed and pointed end, respectively. Except for the detachment rate $\omega_{\text{off},T}^{\text{po}}$, all rates have the same numerical values as those in Table I of Ref. 23. The rate $\omega_{\text{off},T}^{\text{po}}$ is determined by detailed balance in the absence of ATP hydrolysis.

$\kappa_{\text{on},T}^{\text{ba}}$	11.6 ± 0.8
$\kappa_{\text{on},T}^{\text{po}}$	1.3 ± 0.2
$\omega_{\text{off},T}^{\text{ba}}$	1.4
$\omega_{\text{off},T}^{\text{po}}$	0.16
$\omega_{\text{off},\Theta}^{\text{ba}}$	0.2
$\omega_{\text{off},\Theta}^{\text{po}}$	0.02
$\omega_{\text{off},D}^{\text{ba}}$	5.4
$\omega_{\text{off},D}^{\text{po}}$	0.25
ω_c	0.3
ω_r	0.003

B. Transition rates and filament dynamics

The attachment rates $\omega_{\text{on}}^{\text{ba}}$ and $\omega_{\text{on}}^{\text{po}}$ depend on the monomer concentration C_T and on the capture zone sizes d^{ba} and d^{po} . As shown in Ref. 22, these rates have the expected form $\omega_{\text{on}}^{(\alpha)} = \kappa_{\text{on}}^{(\alpha)} C_T$, where the rate constants $\kappa_{\text{on}}^{(\alpha)}$ increase roughly with the third power of the capture zone sizes $d^{(\alpha)}$. In the present study, we have chosen the capture zones $d^{\text{ba}} = 2.5r_0$ and $d^{\text{po}} = 0.903r_0$ where the particle diameter r_0 represents the basic length scale, see Ref. 22. This choice leads to attachment rate constants $\kappa_{\text{on}}^{(\alpha)}$ as deduced experimentally in Ref. 23, see Table I. As mentioned in Sec. I, we consider ‘‘random hydrolysis,’’ for which the rate ω_c for ATP cleavage of a T protomer and the rate ω_r for P_i release from a Θ protomer are both taken to be independent of the local neighborhoods of the T and Θ protomers.

The time evolution of the filament is described as a continuous-time Markov process.²⁷ In order to define the corresponding transitions, we must distinguish the two *terminal* protomers at the barbed and pointed ends from all the other, *internal* protomers as well as the different nucleotide states of both terminal and internal protomers.

Internal D protomers remain unchanged whereas internal T protomers are transformed into Θ protomers, during the time step Δt , with the cleavage probability $P_c = f(\omega_c)$ and $f(z) \equiv 1 - \exp[-z\Delta t]$. Likewise, internal Θ protomers are transformed into D protomers with the phosphate release probability $P_r = f(\omega_r)$. Terminal D protomers at the barbed end detach with probability $P_{\text{off},D}^{\text{ba}} = f(\omega_{\text{off},D}^{\text{ba}})$, which is governed by the detachment rate $\omega_{\text{off},D}^{\text{ba}}$. Terminal T protomers at the barbed end can detach from this end or can be cleaved: They are cleaved with probability $P_c^{\text{ba}} = f(\omega_c + \omega_{\text{off},T}^{\text{ba}}) \pi_c^{\text{ba}}$, which depends on the cleavage rate ω_c , on the detachment rate $\omega_{\text{off},T}^{\text{ba}}$, and on the transition probability $\pi_c^{\text{ba}} \equiv \omega_c / (\omega_c + \omega_{\text{off},T}^{\text{ba}})$, and detach with probability $P_{\text{off},T}^{\text{ba}} = f(\omega_c + \omega_{\text{off},T}^{\text{ba}}) (1 - \pi_c^{\text{ba}})$. Terminal Θ protomers at the barbed end can detach from this end or be transformed into D protomers: They are transformed with probability $P_r^{\text{ba}} = f(\omega_r + \omega_{\text{off},\Theta}^{\text{ba}}) \pi_r^{\text{ba}}$, which depends on the P_i release rate ω_r , on the detachment rate $\omega_{\text{off},\Theta}^{\text{ba}}$, on the transition probability $\pi_r^{\text{ba}} \equiv \omega_r / (\omega_r + \omega_{\text{off},\Theta}^{\text{ba}})$, and detach with probability $P_{\text{off},\Theta}^{\text{ba}} = f(\omega_r + \omega_{\text{off},\Theta}^{\text{ba}}) (1 - \pi_r^{\text{ba}})$.

The time evolution of the terminal protomers at the pointed end is described by completely analogous expressions.

Most simulations reported in this article have been performed using the release rate $\omega_r = 0.003/\text{s}$ as measured in Ref. 25 both for the terminal and for the internal Θ protomers. It has been recently argued, however, that the P_i release rate for a terminal Θ protomer may be different from and much larger than the one for an internal Θ protomer. Therefore, in some simulations, we used a different value for the terminal Θ protomers. The latter value will be explicitly indicated by the symbol $\omega_r(1)$.

C. Detailed balance in the absence of hydrolysis

We will focus on the *in vitro* system in Ref. 23 and, except for the rate $\omega_{\text{off},T}^{\text{po}}$, use the attachment and detachment rates as summarized in Table I of this reference. This *in vitro* system corresponds to Mg-ATP-actin purified from rabbit skeletal muscle and polymerized in a physiological buffer. The detachment rate $\omega_{\text{off},T}^{\text{po}}$, on the other hand, which governs the detachment of T protomers from the pointed end, is chosen in such a way that detailed balance is satisfied in the absence of ATP hydrolysis, compare Ref. 22, in which the same procedure was used for polymerization of ADP-actin monomers. The detailed balance condition implies $\omega_{\text{off},T}^{\text{po}} = \omega_{\text{off},T}^{\text{ba}} \kappa_{\text{on},T}^{\text{po}} / \kappa_{\text{on},T}^{\text{ba}}$.

D. Simulation parameters

In order to obtain a well-defined ensemble of growing (or shrinking) filaments, all filaments are taken to consist of 200 D protomers at the initial time $t=0$ in the cuboidal simulation box of constant volume $V = 30 \times 30 \times 400(r_0)^3$, where r_0 is the basic length scale, which is about 5 nm and corresponds to twice the projected length of one actin protomer.²²

As far as the time scales are concerned, we start from the diffusion of single monomers and then use the rescaling procedure introduced in Ref. 22. First, we define our basic time scale t_{sc} to be equal to the typical time, during which a single monomer in solution undergoes the displacement r_0 by diffusive motion. This implies that $t_{\text{sc}} = r_0^2 / D \approx 0.8 \mu\text{s}$ with the bulk diffusion constant $D \approx 10^{-7} \text{ cm}^2/\text{s}$ of free actin as measured *in vitro*.²⁸ The integration time step Δt for the Brownian dynamics is then taken to be $\Delta t \equiv 10^{-3} t_{\text{sc}} \approx 0.8 \text{ ns}$.

E. Rescaling procedure

Without any rescaling procedure, a rather long simulation of 2.5×10^8 time steps would correspond to 200 ms in real time. The latter time is smaller than the average time between two detachment or attachment events at the two filament ends if the actin concentration is about 0.1 μM , i.e., of the order of the steady state critical concentration as experimentally determined in Refs. 3 and 5. In order to overcome this large separation of time scales between relatively fast monomer diffusion and relatively slow monomer attachment and detachment events, all attachment and detachment processes are speeded up by the same dimensionless factor b . Thus, in the simulations, we use rescaled attachment and detachment rates $\hat{\omega}_{\text{on}}^{(\alpha)} \equiv b \omega_{\text{on}}^{(\alpha)}$ and $\hat{\omega}_{\text{off}}^{(\alpha)} \equiv b \omega_{\text{off}}^{(\alpha)}$.

As explained in Ref. 22, our rescaling procedure is defined in such a way (i) that the ratio of the rescaled attachment rate constants $\hat{\kappa}_{\text{on}}$ is equal to the ratio of the measured attachment rate constants κ_{on} , and (ii) that the size of the capture zones at the two filament ends is comparable to the size of a free actin monomer. These two requirements imply that we increase the actin monomer concentration C_T by a certain rescaling factor b_C and use the rescaled concentration $\hat{C}_T \equiv b_C C_T$ in the simulations. In the present study, the rescaling factors had the values $b=5000$ and $b_C=812$.

As far as filament polymerization and depolymerization are concerned, the real system at time t then corresponds to the simulated system at time $\hat{t}=t/b$. The only drawback of this rescaling procedure is that the diffusive motion of the actin monomers is now too slow compared to the attachment and detachment processes, which imply that newly detached monomers would reattach too frequently to the filament. In order to avoid these enhanced reattachment events, we remove the newly detached monomers from the solution²² which also ensures that the monomer concentration remains unchanged.

III. RESULTS AND DISCUSSION

Because of the stochastic nature of the different processes involved in the coupling of actin polymerization and ATP hydrolysis, rather long simulations are required in order to estimate the different quantities in a reliable way. Indeed, the average quantities discussed in this section have been typically obtained by averaging over an ensemble of many filaments, each of which has been simulated for more than 2×10^8 time steps.

A. Growth rates and concentration regimes

First, we consider the overall growth rate J_g of a filament. This quantity represents the average number of monomers, by which the filament length L is increased per unit time. Therefore, this growth rate can be determined from the relation $J_g = \frac{d}{dt} \langle L \rangle$ by measuring the average filament length $\langle L \rangle$ as a function of time t . This method has been used to obtain the functional dependence of J_g on the free actin concentration C_T as shown in Fig. 2. In this figure, each data point depicted as a black square has been calculated by averaging over 20 growing filaments. The same figure also displays another set of data points, the red stars, which were obtained by measuring the average binding and unbinding times at the two filament ends, see further below. Inspection of Fig. 2 shows that the rate J_g is negative for small C_T , positive for large C_T , and vanishes at the critical concentration $C_T = C_{T,\text{cr}}$. The latter concentration is often called the steady state critical concentration³ because the filament attains a constant average length at $C_T = C_{T,\text{cr}}$. The data obtained via $J_g = \frac{d}{dt} \langle L \rangle$ lead to the estimate $C_{T,\text{cr}} \approx 0.064 \mu\text{M}$, see Fig. 2, for the transition rates in Table I. This value for the critical concentration is consistent with the experimentally determined values as reported in Refs. 3 and 5.

The overall growth rate J_g can be decomposed into two contributions from the two filament ends according to

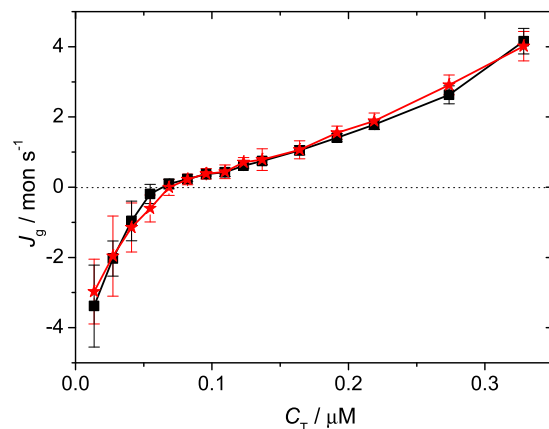


FIG. 2. The overall growth rate J_g as a function of free actin concentration C_T . The two different sets of data have been obtained by measuring the average filament length (black squares) and the average waiting times between successive attachment and detachment events (red stars) as explained in the text. The transition rates are the same as in Table I.

$$J_g = J_g^{\text{ba}} + J_g^{\text{po}}. \quad (1)$$

Both growth rates J_g^{ba} and J_g^{po} are measured in units of monomers per second or mon/s. Depending on the free actin monomer concentration, each of these rates can be positive or negative corresponding to a growing or shrinking filament end. At the critical concentration, $C_T = C_{T,\text{cr}}$ with $J_g = 0$, one has $J_g^{\text{ba}} = -J_g^{\text{po}}$. For $C_T < C_{T,\text{cr}}$, the overall growth rate J_g is negative whereas it is positive for $C_T > C_{T,\text{cr}}$.

In general, the growth rate J_g^{ba} of the barbed end may be positive or negative at the critical concentration $C_T = C_{T,\text{cr}}$. For the transition rates as given in Table I, we conclude from our simulations that J_g^{ba} is positive at $C_T \approx C_{T,\text{cr}}$, which implies that the barbed end grows whereas the pointed end shrinks. The low concentration regime $C_T < C_{T,\text{cr}}$ is then further subdivided into two subregimes by a second critical concentration, $C_{T,\text{cr}}^{\text{ba}}$, at which the growth rate J_g^{ba} of the barbed end vanishes. In the subregime with $C_T < C_{T,\text{cr}}^{\text{ba}}$, both the pointed and the barbed end are shrinking, although with different rates. Indeed, for very low concentrations, the filament consists only of D protomers and the barbed end is shrinking with the detachment rate $\omega_{\text{off},D}^{\text{ba}} = 5.4/\text{s}$ while the pointed end is shrinking with the relatively small rate $\omega_{\text{off},D}^{\text{po}} = 2.5/\text{s}$. In the subregime with $C_{T,\text{cr}}^{\text{ba}} < C_T < C_{T,\text{cr}}$, the filament still undergoes treadmilling in the sense that the barbed end grows and the pointed end shrinks but the pointed end shrinks faster than the barbed end grows.

Likewise, the high concentration regime $C_T > C_{T,\text{cr}}$ is also subdivided into two subregimes by a third critical concentration, $C_{T,\text{cr}}^{\text{po}}$, at which the growth rate J_g^{po} of the pointed end vanishes. For $C_{T,\text{cr}} < C_T < C_{T,\text{cr}}^{\text{po}}$, the barbed end grows and the pointed end shrinks but the barbed end grows faster than the pointed end shrinks. Finally, for $C_T > C_{T,\text{cr}}^{\text{po}}$, both filament ends exhibit a positive growth rate. Indeed, for very high concentrations, the terminal protomers are in the T state and the barbed end grows with the attachment rate $\omega_{\text{on},T}^{\text{ba}} = (11.6/\text{s}) \times (C_T / \mu\text{M})$ while the pointed end grows with the attachment rate $\omega_{\text{on},T}^{\text{po}} = (1.3/\text{s}) \times (C_T / \mu\text{M})$.

Therefore, for the transition rates in Table I, the overall growth rate J_g of the filament is dominated by the growth

rate J_g^{ba} of the barbed end *both* for shrinking filaments at low concentrations, for which $J_g^{ba} < 0$, and for growing filaments at high concentrations, for which $J_g^{ba} > 0$. In fact, our simulations show that $|J_g^{ba}| \gg |J_g^{po}|$ for all concentrations apart from a small concentration regime around the critical concentration $C_{T,cr}$.

This asymmetry between the barbed and the pointed end also implies that the barbed end critical concentration $C_{T,cr}^{ba}$ and the pointed end critical concentration $C_{T,cr}^{po}$ have numerical values that are quite close to the value of the steady state critical concentration $C_{T,cr} \approx 0.064 \mu\text{M}$. Indeed, our simulations lead to the estimates $C_{T,cr}^{ba} \approx 0.063$ and $C_{T,cr}^{po} \approx 0.072$. This similarity of the critical concentrations at the two ends has also been observed in the stochastic simulations of Ref. 17.

B. Treadmilling rate: Single filament simulations

The growth rates J_g^{ba} and J_g^{po} at the two filament ends are intimately related to the average velocities $\langle v^{ba} \rangle$ and $\langle v^{po} \rangle$ of these two ends. We use the convention that the velocity $\langle v^{ba} \rangle$ and the growth rate J_g^{ba} of the barbed end have the same sign, while the velocity $\langle v^{po} \rangle$ and the growth rate J_g^{po} of the pointed end have opposite signs. Thus, in the concentration regime $C_{T,cr}^{ba} < C_T < C_{T,cr}^{po}$, the velocities of both ends are positive corresponding to a growing barbed end and a shrinking pointed end. The treadmilling velocity v_{tm} is then given by

$$v_{tm} \equiv \frac{1}{2}(\langle v^{ba} \rangle + \langle v^{po} \rangle) \quad (2)$$

which is also positive in the whole treadmilling regime with $C_{T,cr}^{ba} < C_T < C_{T,cr}^{po}$.

Since the protomer extension parallel to the filament is $r_0/2$ as in Ref. 22, the average velocities of the filament ends can be estimated by $\langle v^{ba} \rangle \approx J_g^{ba} r_0/2$ and $\langle v^{po} \rangle \approx -J_g^{po} r_0/2$, where we have ignored small corrections arising from the translational diffusion and the shape fluctuations of the filament. This implies that the treadmilling velocity can also be estimated by $v_{tm} \approx J_{tm} r_0/2$ with the treadmilling rate J_{tm} defined by

$$J_{tm} \equiv \frac{1}{2}(J_g^{ba} - J_g^{po}) \quad (3)$$

which is again positive for $C_{T,cr}^{ba} < C_T < C_{T,cr}^{po}$.

One example for treadmilling as observed in the simulations for free actin concentration $C_T = 0.064 \mu\text{M}$, close to the critical concentration $C_{T,cr}$, is shown in Fig. 3. The filament length L strongly fluctuates with time t but its average value is approximately constant. In contrast, the positions of the two filament ends both move, on average, toward positive x -values, see Fig. 3. For the two trajectories displayed in this figure, the average velocities $\langle v^{ba} \rangle$ and $\langle v^{po} \rangle$ of the two filament ends are roughly equal to $\langle v^{ba} \rangle \approx \langle v^{po} \rangle \approx 0.035 r_0/s$. Using the expression (2), we then obtain the rough estimates $v_{tm} \approx 0.035 r_0/s$ for the treadmilling velocity and $J_{tm} \approx 0.07 \text{ mon/s}$ for the treadmilling rate, where mon/s stands for ‘‘monomers per second.’’

The time interval of 1400 s as depicted in Fig. 3 corresponds to a rather long simulation time of 3.5×10^8 time

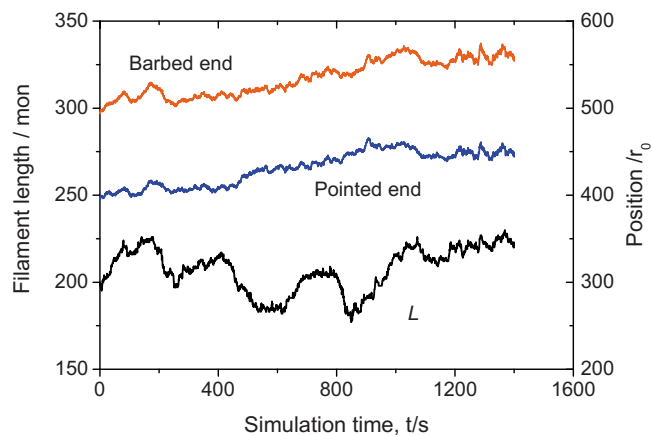


FIG. 3. Filament length L and positions of barbed and pointed end as functions of simulation time t . The length L is measured in units of protomer number (left y-axis), the end positions are measured in units of the basic length scale r_0 (right y-axis). The filament grows parallel to the long side of the simulation box, which has an extension of $400r_0$, the longitudinal extension of one protomer is $r_0/2$. The transition rates are the same as in Table I, the free actin concentration is $C_T = 0.064 \mu\text{M}$ close to the critical concentration $C_{T,cr}$.

steps Δt . As shown in this figure, treadmilling implies a random walk of the filament length characterized by large excursions from the average value $\langle L \rangle$. Averaging over more than ten trajectories as shown in this figure, the growth rate J_g is estimated to be $J_g = \frac{d}{dt} \langle L(t) \rangle \approx 0.015 \text{ mon/s}$ for $C_T = 0.064 \mu\text{M}$.

C. Treadmilling rate: On-off statistics at filament ends

The attachment and detachment events at the (α) end of the filament can also be characterized by the average attachment and detachment times, $\tau_{on}^{(\alpha)}$ and $\tau_{off}^{(\alpha)}$. These time scales are obtained from histograms as in Fig. 4. The latter example corresponds to free actin concentration $C_T = 0.064 \mu\text{M}$ close to the critical concentration $C_{T,cr}$. The left panels in Figs. 4(a) and 4(b) show the measured attachment times $t_{on}^{(\alpha)}$ between two successive attachment events at the barbed and pointed end; the right panels the measured detachment times $t_{off}^{(\alpha)}$ between two successive detachment events at these two ends. The average attachment times $\tau_{on}^{(\alpha)} = \langle t_{on}^{(\alpha)} \rangle$ and the average detachment time $\tau_{off}^{(\alpha)} = \langle t_{off}^{(\alpha)} \rangle$ are then calculated in two ways: (i) by direct summation over the histograms and (ii) by exponential fits to these histograms. For simplicity, we fitted the data to single exponentials even though the detachment events involve several time scales. In this way, we obtain the estimates $\tau_{on}^{ba} = 1.34 \pm 0.03$, $\tau_{off}^{ba} = 1.59 \pm 0.06$, $\tau_{on}^{po} = 11.2 \pm 0.6$, and $\tau_{off}^{po} = 7.4 \pm 2.1$ for the data in Fig. 4 corresponding to $C_T = 0.064 \mu\text{M}$. The value for the average detachment time τ_{off}^{po} has a relatively large error reflecting the noisy data in Fig. 4(b).

From the attachment and detachment times, we can calculate the growth rates J_g^{ba} and J_g^{po} of the two filament ends via

$$J_g^{(\alpha)} = 1/\tau_{on}^{(\alpha)} - 1/\tau_{off}^{(\alpha)} \quad (4)$$

as well as the overall growth rate $J_g = J_g^{ba} + J_g^{po}$ as in Eq. (1) and the treadmilling rate $J_{tm} = \frac{1}{2}(J_g^{ba} - J_g^{po})$ as in Eq. (3). In this

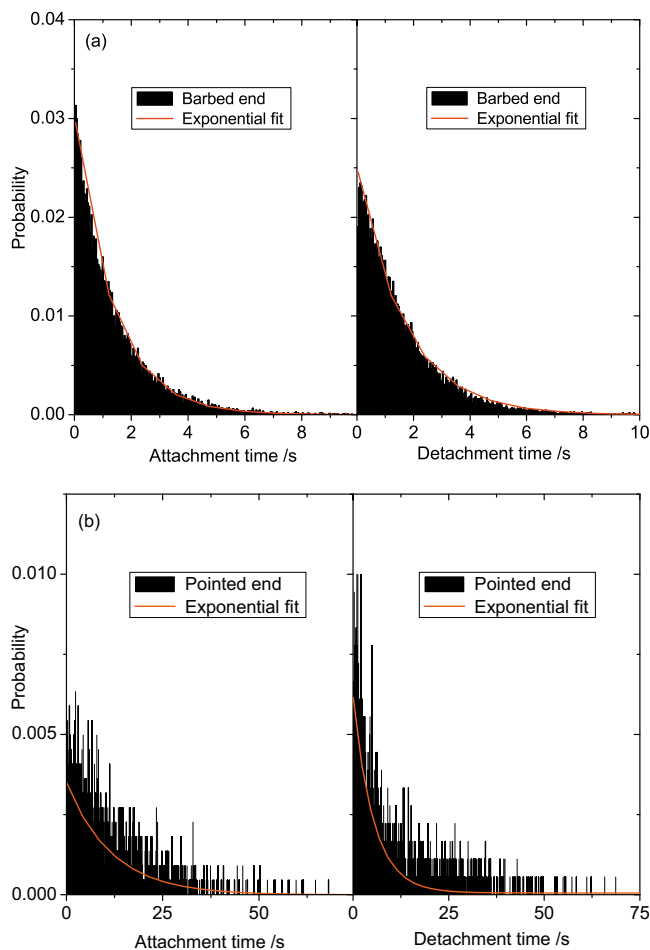


FIG. 4. Normalized histograms for time intervals between two successive monomer attachments and two successive protomer detachments at the (a) barbed and (b) pointed end. The parameters are the same as in Fig. 3.

way, we obtained the J_g -values corresponding to the red stars in Fig. 2. For $C_T=0.064 \mu\text{M}$, the average waiting times deduced from the data in Fig. 4 lead to the overall growth rate $J_g \approx 0.06 \text{ mon/s}$ and the treadmilling rate $J_{tm} \approx 0.08 \text{ mon/s}$.

D. State probabilities of terminal protomers

In the steady state, each end of a growing filament can be characterized by the three probabilities $P_T^{(\alpha)}(1)$, $P_\Theta^{(\alpha)}(1)$, and $P_D^{(\alpha)}(1)$ that the terminal protomer at the (α) end is in its T , Θ and D state, respectively.¹⁹ As shown in Fig. 5, these probabilities exhibit a strong dependence on the free actin concentration C_T . In the limit of large C_T , the filament grows continuously at both ends, and the terminal protomers represent recently attached T monomers, which leads to $P_T^{(\alpha)}(1) \approx 1$ for large C_T . For small actin concentration C_T , on the other hand, the depolymerizing filament consists only of D protomers, which imply that $P_D^{(\alpha)}(1) \approx 1$ for small C_T . Since $P_D^{(\alpha)}(1) + P_\Theta^{(\alpha)}(1) + P_T^{(\alpha)}(1) = 1$, the probability $P_\Theta^{(\alpha)}(1)$ to find a terminal protomer in the Θ state must vanish both for small and for large C_T and, thus, must have a maximum at an intermediate C_T -value. This nonmonotonic behavior of $P_\Theta^{(\alpha)}(1)$ is clearly visible in Figs. 5(a) and 5(b), which display the data for the barbed and pointed end, respectively. In both

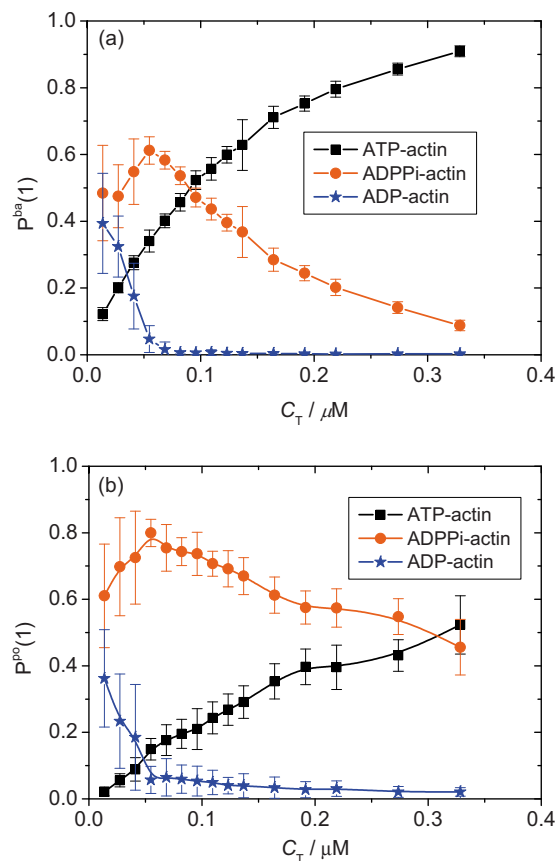


FIG. 5. The three probabilities $P_Y^{ba}(1)$ with $Y=T, \Theta$, and D for the terminal protomer at the (a) barbed and (b) pointed end as a function of free actin concentration C_T . The transition rates are the same as in Table I.

cases, the concentration, at which $P_\Theta^{(\alpha)}(1)$ attains its maximum, is close to the critical concentration $C_{T,cr}^{(\alpha)}$ of the (α) end.

If the concentration exceeds the critical concentration $C_{T,cr} \approx 0.064$, the probabilities $P_D^{ba}(1)$ and $P_D^{pp}(1)$ to find the terminal protomers at the barbed or pointed end in the D state are quite small as shown in Fig. 5. Below the critical concentration, the probabilities $P_D^{(\alpha)}(1)$ increase monotonically with decreasing C_T and attain the limiting value $P_D^{(\alpha)}(1) = 1$ for $C_T = 0$. Therefore, the detachment rate of the D protomer is expected to have only a small influence on the value of the critical concentration. This expectation was confirmed by three sets of simulations corresponding to three different values of the detachment rate $\omega_{off,D}^{ba}$ of the D protomer at the barbed end as shown in Fig. 6.

E. Phosphate release from terminal protomers

It has been recently argued²³ that the P_i release rate ω_r for a terminal Θ protomer satisfies $\omega_r \geq 2/s$, which is much larger than the P_i release rate $\omega_r = 0.003/s$ for an internal Θ protomer. In order to study the effect of increased P_i release from the terminal protomers, we have performed simulations for three different cases: (I) Both internal and terminal protomers have the same P_i release rate $\omega_r = 0.003/s$; (II) The release rate $\omega_r = 0.003/s$ for an internal protomer but $\omega_r(1) = 2/s$ for a terminal protomer; and (III) Both terminal and internal protomers are characterized by $\omega_r = 2/s$. The corre-

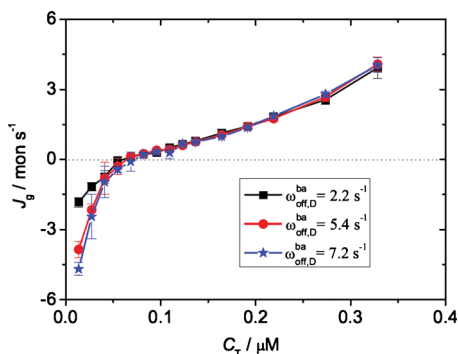


FIG. 6. Overall growth rate J_g as a function of free actin concentration C_T for three different values of the rate $\omega_{\text{off},D}^{\text{ba}}$, which governs the detachment of D protomers from the barbed end. The other transition rates have the same values as in Table I.

sponding data for the overall growth rate J_g are displayed in Fig. 7, which shows that the critical concentration $C_{T,\text{cr}}$ varies from the value $C_{T,\text{cr}} \approx 0.06 \mu\text{M}$ for case (I) over $C_{T,\text{cr}} \approx 0.13 \mu\text{M}$ for case (II) to $C_{T,\text{cr}} \approx 0.17 \mu\text{M}$ for case (III). This shift of the critical concentration can be understood as follows.

First, we note that the growth rate $J_g^{(\alpha)}$ of the (α) end is directly related to the probabilities $P_Y^{(\alpha)}(1)$ with $Y=T, \Theta$, and D and can be expressed as

$$J_g^{(\alpha)} = \kappa_{\text{on}}^{(\alpha)} C_T - \sum_Y P_Y^{(\alpha)}(1) \omega_{\text{off},Y}^{(\alpha)}, \quad (5)$$

where the summation runs over the three nucleotide states $Y=T, \Theta$, and D . The first term proportional to C_T represents the attachment flux onto the filament end (α) whereas the second term corresponds to the total detachment flux from this filament end. At the critical concentration, the overall flux vanishes, i.e., $J_g^{\text{ba}} + J_g^{\text{po}} = 0$. Using relation (5), this flux balance attains the form

$$(\kappa_{\text{on}}^{\text{ba}} + \kappa_{\text{on}}^{\text{po}}) C_{T,\text{cr}} = \sum_Y [P_Y^{\text{ba}}(1) \omega_{\text{off},Y}^{\text{ba}} + P_Y^{\text{po}}(1) \omega_{\text{off},Y}^{\text{po}}]. \quad (6)$$

The sum on the right hand side of this equation represents the total detachment flux of protomers from both ends of the filament.

Next, let us consider case (I) at the corresponding critical concentration $C_{T,\text{cr}} = C_{T,\text{cr}}^{(I)}$. Such a system is characterized by

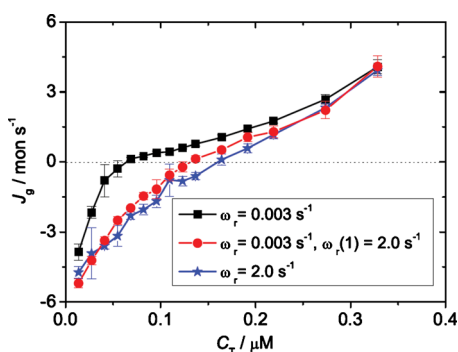


FIG. 7. Overall growth rate J_g as a function of free actin concentration C_T for three different choices of the P_i release rates ω_r and $\omega_r(1)$, which govern the internal and terminal Θ protomers, respectively. The values of all other transition rates are in Table I.

large probabilities $P_{\Theta}^{(\alpha)}(1)$ to find the terminal protomers in the Θ state but small probabilities $P_D^{(\alpha)}(1)$ to find them in the D state, see Fig. 5. If we now increase the P_i release rates ω_r of the terminal protomers, these protomers are more likely to be in the D state, i.e., we increase the probabilities $P_D^{(\alpha)}(1)$ and decrease the probabilities $P_{\Theta}^{(\alpha)}(1)$. Since $\omega_{\text{off},D}^{(\alpha)} \gg \omega_{\text{off},\Theta}^{(\alpha)}$ both at the barbed and at the pointed end, see Table I, the change in the total detachment flux on the right hand side of Eq. (6) is dominated by the increase of $P_D^{(\alpha)}(1)$, which implies an increasing total detachment flux and a shrinking filament. Therefore, we conclude that an increase in the release rates ω_r for the terminal protomers leads to an increase in the critical concentration.

F. Steady state protomer patterns

If we follow the time evolution of this growing filament for a sufficiently long time, the protomer pattern at the (α) end attains a steady state as described by three time-independent density profiles $P_T^{(\alpha)}(x_\alpha)$, $P_{\Theta}^{(\alpha)}(x_\alpha)$, and $P_D^{(\alpha)}(x_\alpha)$ where the spatial coordinate x_α measures the distance from the (α) end at $x_\alpha \equiv 1$ in units of the projected protomer length.¹⁹ Thus, in order to determine the steady state protomer pattern at the (α) end, we need to use a comoving coordinate system, in which the terminal protomer at the (α) end has a fixed position. At the critical concentration $C_{T,\text{cr}}$, the average velocity of the pointed end, $\langle v^{\text{po}} \rangle$, is equal to the average velocity of the barbed end, $\langle v^{\text{ba}} \rangle$, see Fig. 3. We can then observe the steady state protomer patterns at both ends simultaneously using a coordinate system that moves with constant velocity $\langle v^{\text{ba}} \rangle = \langle v^{\text{po}} \rangle$. More precisely, we can determine these patterns if the filaments are sufficiently long, and one can ignore the overlap of the protomer density profiles from the two ends.

For monomer concentrations C_T that exceed the critical concentration $C_{T,\text{cr}}$, the average length of the filament grows and the barbed end moves faster than the pointed end, i.e., $\langle v^{\text{ba}} \rangle > \langle v^{\text{po}} \rangle$. In this case, we have to use two different comoving coordinate systems in order to observe the steady state protomer patterns at the two filament ends. Finally, for $C_T < C_{T,\text{cr}}$, the average filament length shrinks and the protomer density profiles will always start to overlap eventually. Therefore, in the latter case, the protomer patterns at the two filament ends cannot attain a true steady state.

Since we started from a certain initial pattern, in which all protomers are in the D state, we had to perform sufficiently long simulation runs in order to reach the steady state protomer patterns at the two filament ends. One example for the protomer density profiles obtained in this way is displayed in Fig. 8 corresponding to $C_T = 0.064 \mu\text{M}$, which is close to the critical concentration $C_{T,\text{cr}}$. As shown in this figure, the steady state protomer pattern is characterized by a very short T cap and an extended Θ segment at the barbed end as well as some intercalated Θ protomers at the pointed end. As one increases the free actin concentration C_T , the protomer density profiles attain longer T caps and even more extended Θ segments but still exhibit the same qualitative features as those visible in Fig. 8.

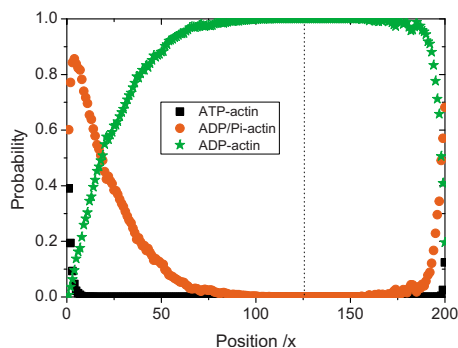


FIG. 8. The density profiles P_Y^{ba} (left) and P_Y^{po} (right) for $Y=T, \Theta$, and D protomers as a function of the spatial coordinate $x \equiv x_{ba} \equiv 201 - x_{po}$ where x is measured in units of the projected protomer size. The barbed end is located at $x=x_{ba}=1$, the pointed end at $x_{po}=1$ or $x=200$. The values of the transition rates are given in Table I; the free actin concentration is $C_T = 0.064 \mu\text{M}$.

Using the density profile $P_T^{(\alpha)}(x_\alpha)$, one can obtain the average number $\langle N_T^{(\alpha)} \rangle$ of T protomers at the (α) end via

$$\langle N_T^{(\alpha)} \rangle = \sum_{x_\alpha=1} P_T^{(\alpha)}(x_\alpha), \quad (7)$$

where the summation extends up to x_α -values for which $P_T^{(\alpha)}(x_\alpha)$ has essentially decayed to zero. Likewise, the average number $\langle N_\Theta^{(\alpha)} \rangle$ of Θ protomers at the (α) end is given by

$$\langle N_\Theta^{(\alpha)} \rangle = \sum_{x_\alpha=1} P_\Theta^{(\alpha)}(x_\alpha), \quad (8)$$

where the summation extends up to x_α -values for which $P_\Theta^{(\alpha)}(x_\alpha)$ has essentially decayed to zero. Using the expressions (7) and (8) for the density profiles as shown in Fig. 8, the T and Θ segments at the barbed end have the average extensions $\langle N_T^{ba} \rangle \approx 0.77$ and $\langle N_\Theta^{ba} \rangle \approx 22.73$ protomers, while the segments at the pointed end are shorter with $\langle N_T^{po} \rangle \approx 0.13$ and $\langle N_\Theta^{po} \rangle \approx 5.28$ protomers.

G. Flux balance relations

In addition to the density profiles $P_Y^{(\alpha)}(x_\alpha)$, the steady state of the two filament ends can also be characterized by the flux profiles $j_c^{(\alpha)}(x_\alpha)$ for ATP cleavage and $j_r^{(\alpha)}(x_\alpha)$ for P_i release. For random cleavage and release processes as considered here, these flux profiles can be expressed in terms of the density profiles $P_T^{(\alpha)}(x_\alpha)$ and $P_\Theta^{(\alpha)}(x_\alpha)$ for T and Θ protomers. Indeed, the ATP cleavage flux profile has the form

$$j_c^{(\alpha)}(x_\alpha) = P_T^{(\alpha)}(x_\alpha) \omega_c \quad (9)$$

and the P_i release flux profile is given by

$$j_r^{(\alpha)}(x_\alpha) = P_\Theta^{(\alpha)}(x_\alpha) \omega_r. \quad (10)$$

These flux profiles can be used to calculate the total ATP cleavage flux

$$J_c^{(\alpha)} \equiv \sum_{x_\alpha=1} j_c^{(\alpha)}(x_\alpha) \quad (11)$$

and the total P_i release flux

$$J_r^{(\alpha)} \equiv \sum_{x_\alpha=1} j_r^{(\alpha)}(x_\alpha) \quad (12)$$

at the (α) end of the filament. Inserting the expressions (9) and (10) for the flux profiles into the expressions (11) and (12), respectively, as well as using the relations (7) and (8) for the average numbers of T and Θ protomers, we obtain the two flux balance relations

$$J_c^{(\alpha)} = \langle N_T^{(\alpha)} \rangle \omega_c \quad \text{and} \quad J_r^{(\alpha)} = \langle N_\Theta^{(\alpha)} \rangle \omega_r, \quad (13)$$

for the total cleavage flux $J_c^{(\alpha)}$ and the total P_i release flux $J_r^{(\alpha)}$ at the (α) end.

In the steady state, the total cleavage flux $J_c^{(\alpha)}$ and the total P_i release flux $J_r^{(\alpha)}$ at the (α) end must satisfy the flux balance condition

$$J_c^{(\alpha)} = J_r^{(\alpha)} + P_\Theta^{(\alpha)}(1) \omega_{\text{off}, \Theta}^{(\alpha)}. \quad (14)$$

Using this latter condition together with Eq. (13), one obtains the relation

$$\langle N_T^{(\alpha)} \rangle \omega_c = \langle N_\Theta^{(\alpha)} \rangle \omega_r + P_\Theta^{(\alpha)}(1) \omega_{\text{off}, \Theta}^{(\alpha)} \quad (15)$$

between the average numbers $\langle N_T^{(\alpha)} \rangle$ and $\langle N_\Theta^{(\alpha)} \rangle$ of the T and Θ protomers at the (α) end.

For $C_T = 0.064 \mu\text{M}$, the barbed end is characterized by $\langle N_T^{ba} \rangle \approx 0.77$ and $\langle N_\Theta^{ba} \rangle \approx 22.73$ as deduced from the data displayed in Fig. 8 as well as by $P_\Theta^{ba}(1) \approx 0.62$, see Fig. 5(a). Inserting these numerical values into the flux balance relation (15), we then obtain the fluxes 0.23 and 0.19 mon/s for the left and right hand side of this equation, respectively. Likewise, for the pointed end at $C_T = 0.064 \mu\text{M}$, we obtained $\langle N_T^{po} \rangle \approx 0.13$ and $\langle N_\Theta^{po} \rangle \approx 5.28$ as well as $P_\Theta^{po}(1) \approx 0.80$, see Fig. 5(b). Inserting these values into the flux balance relation (15), we obtain the fluxes 0.039 and 0.032 mon/s for the left and right hand side of this equation. Therefore, the flux balance relation (15) is fulfilled with an accuracy of about 10% at the barbed end and with an accuracy of about 20% at the pointed end.

IV. CONCLUSIONS

In summary, we have presented the first particle-based computer simulations of ATP-actin polymerization and of the associated treadmilling process. For the transition rates as given in Table I, which satisfy detailed balance in the absence of ATP hydrolysis, the steady state critical concentration was found to be $C_{T,cr} \approx 0.064 \mu\text{M}$, see Fig. 2. This value is consistent with the experimentally deduced value $C_{T,cr} \approx 0.1 \mu\text{M}$ as reported in Refs. 3 and 5. We were also able (i) to observe the treadmilling process in long simulation runs as shown in Fig. 3 and (ii) to estimate the corresponding treadmilling (or turnover) rate from the on-off statistics at the two filament ends, see Fig. 4, which leads to the value $J_{tm} \approx 0.08$ mon/s for $C_T = 0.064$. This value for J_{tm} corresponds to the turnover of a $2.4 \mu\text{m}$ long filament in 3 h. This value is rather small but consistent with the treadmilling rate $J_{tm} \approx 0.1$ mon/s as deduced from the experiments in Ref. 29.

Furthermore, we investigated several other quantities and relations that are difficult to study experimentally but

provide nontrivial crosschecks on the consistency of our simulations: (i) the probabilities for the terminal protomers at the two filament ends to be in different nucleotide states, see Fig. 5; (ii) the density and flux profiles along the filament, see Fig. 8 as well as relations (9) and (10); (iii) the average numbers of ATP-actin and ADP/P_i-actin protomers as found at the two filament ends in the steady state, which can be calculated via the expressions (7) and (8); and (iv) the flux balance relation (15).

We have also studied the dependence of the steady state critical concentration $C_{T,cr}$ on the detachment rate $\omega_{off,D}$ for D protomers at the barbed end, see Fig. 6, as well as on the P_i release rate ω_r , see Fig. 7. We found that the critical concentration $C_{T,cr}$ is hardly affected when the detachment rate $\omega_{off,D}$ is varied from 2.2 to 7.2 mon/s. On the other hand, if we use the enhanced P_i release $\omega_r(1)=2/s$ for the terminal protomers as proposed in Ref. 23, we find that the value of the critical concentration is increased from $C_{T,cr} \approx 0.06 \mu\text{M}$ to $0.13 \mu\text{M}$, see Fig. 7.

Our particle-based simulation approach can be extended to study a variety of more complex systems. One interesting target for future simulation studies is provided by the activity of actin-binding proteins such as actin depolymerization factor, which is known to increase the polymerization from pointed end and to enhance the treadmilling rate by a factor of about 25.²⁹ Likewise, our simulation approach can be used to study the influence of external forces on growing filaments or filament bundles as well as the confining effects of walls and more complex geometries, for which some of the filament ends may be partially shielded from the diffusing monomers.

ACKNOWLEDGMENTS

Kunkun Guo thanks Professor Dong Qiu and Xin Li for stimulating discussions and acknowledges financial support by BNLMS and NSFC (Grant Nos. 10947177 and 21004018). Julian Shillcock was supported by the Danish National Research Foundation via MEMPHYS.

- ¹D. Bray, *Cell Movements* (Garland, New York, 2001).
- ²H. Lodish, A. Berk, C. A. Kaiser, M. Krieger, M. P. Scott, A. Bretscher, H. Ploegh, and P. Matsudaira, *Molecular Cell Biology*, 6th ed. (Freeman, San Francisco, 2007).
- ³D. Pantaloni, C. L. Clainche, and M. F. Carlier, *Science* **292**, 1502 (2001).
- ⁴T. D. Pollard and G. G. Borisy, *Cell* **112**, 453 (2003).
- ⁵T. D. Pollard and A. G. Weeds, *FEBS Lett.* **170**, 94 (1984).
- ⁶M. F. Carlier and D. Pantaloni, *Biochemistry* **25**, 7789 (1986).
- ⁷T. D. Pollard, *J. Cell Biol.* **103**, 2747 (1986).
- ⁸E. D. Korn, M. F. Carlier, and D. Pantaloni, *Science* **238**, 638 (1987).
- ⁹A. Wegner, *J. Mol. Biol.* **108**, 139 (1976).
- ¹⁰Note that the term "critical concentration," which is standard terminology in the research field of actin polymerization, does not imply any critical point corresponding to a continuous phase transition.
- ¹¹A. van Oudenaarden and J. A. Theriot, *Nat. Cell Biol.* **1**, 493 (1999); J. van der Gucht, E. Paluch, J. Plastino, and C. Sykes, *Proc. Natl. Acad. Sci. U.S.A.* **102**, 7847 (2005).
- ¹²I. Fujiwara, S. Takahashi, H. Tadakuma, T. Funatsu, and S. Ishiwata, *Nat. Cell Biol.* **4**, 666 (2002).
- ¹³D. Pantaloni, T. Hill, M.-F. Carlier, and E. Korn, *Proc. Natl. Acad. Sci. U.S.A.* **82**, 7207 (1985).
- ¹⁴A. Mogilner and G. Oster, *Biophys. J.* **71**, 3030 (1996); **84**, 1591 (2003); *Science* **302**, 1340 (2003).
- ¹⁵M. Bindschadler, E. A. Osborn, C. F. Dewey, and J. L. McGrath, *Biophys. J.* **86**, 2720 (2004).
- ¹⁶E. B. Stukalin and A. B. Kolomeisky, *Biophys. J.* **90**, 2673 (2006).
- ¹⁷D. Vavylonis, Q. B. Yang, and B. O. Shaughnessy, *Proc. Natl. Acad. Sci. U.S.A.* **102**, 8543 (2005).
- ¹⁸J. Fass, C. Pak, J. Bamburg, and A. Mogilner, *J. Theor. Biol.* **252**, 173 (2008).
- ¹⁹X. Li, Y. Kierfeld, and R. Lipowsky, *Phys. Rev. Lett.* **103**, 048102 (2009).
- ²⁰D. Sept, A. H. Elcock, and J. A. McCammon, *J. Mol. Biol.* **294**, 1181 (1999).
- ²¹D. Sept and J. A. McCammon, *Biophys. J.* **81**, 667 (2001).
- ²²K. K. Guo, J. C. Shillcock, and R. Lipowsky, *J. Chem. Phys.* **131**, 015102 (2009).
- ²³I. Fujiwara, D. Vavylonis, and T. D. Pollard, *Proc. Natl. Acad. Sci. U.S.A.* **104**, 8827 (2007).
- ²⁴M.-F. Carlier, D. Pantaloni, and E. Korn, *J. Biol. Chem.* **262**, 3052 (1987).
- ²⁵R. Melki, S. Fievez, and M.-F. Carlier, *Biochemistry* **35**, 12038 (1996).
- ²⁶T. Ohm and A. Wegner, *Biochim. Biophys. Acta* **1208**, 8 (1994).
- ²⁷N. G. Van Kampen, *Stochastic Processes in Physics and Chemistry*, 3rd ed. (Elsevier, Amsterdam, 2007).
- ²⁸J. L. McGrath and Y. Tardy, *Biophys. J.* **75**, 2070 (1998).
- ²⁹D. Didry, M. F. Carlier, and D. Pantaloni, *J. Biol. Chem.* **273**, 25602 (1998).